leads to an attempt to use new approaches to solving the problem of deformation of a material with a crack. The effect of loading-cycle length on plastic-zone kinetics obtained by means of the dislocation model for plastic deformation described in the work agrees on the whole with observations in direct experiments. In addition, the closed system occurring in the process of solution for intermediate results of the map for unlike dislocation density $\Delta\delta(\mathbf{r})$ and maps for the overall dislocation density taking part in the plastic deformation process, and also distribution of operating residual stresses (which are distantly operating stress fields for an assembly of unlike dislocations) may be used in building physically equiprobable dislocation models of fatigue crack growth.

The difference in the approach suggested for studying fatigue failure from semiempirical theories existing in linear fracture mechanics includes the following. Absence of a physical base in mathematical models of semiempirical theories induces mechanical engineers to limit themselves to one or two parameters of the number which affect crack extension rate. In the opposite case the number of empirical constants in resulting expressions increases nonlinearly. The approach described in this work makes it possible to build on the basis of a dislocation model a multiparameter relationship for $d\alpha/dN$ with a limited number of empirical constants.

LITERATURE CITED

1. R. Honeycombe, Plastic Deformation of Metals [Russian translation], Mir, Moscow (1972).
2. V. R. Regel', A. I. Slutsker, and É. E. Tomashevskii, Kinetic Strength Theory for Solids [in Russian], Nauka, Moscow (1974).
3. V. I. Vladimirov, A. N. Karpinskii, et al., "Modeling in a computer deformation kinetics in the plastic zone at a crack tip," Probl. Prochn., No. 12 (1983).
4. V. I. Vladimirov, The Physical Nature of Metal Failure [in Russian], Metallurgiya, Moscow (1984).

THREE-DIMENSIONAL BENDING GRAVITATIONAL OSCILLATIONS NEAR MOVING PRESSURE REGIONS

A. E. Bukatov and V. V. Zharkov

UDC 532.593:539.3:624.131

Three-dimensional bending gravitational waves, excited in the near zone during the motion of constant pressure regions over a uniformly compressed thin elastic film, floating on the surface of a homogeneous ideal incompressible fluid of finite depth, are investigated within the linear theory. The dependence of the structure of oscillations on the velocity of the displaced pressure region, film thickness, and magnitude of compressing force is analyzed.

The asymptotic analysis of development of bending gravitational waves was carried out in [1, 2] for motion of a planar pressure front, and in [1, 3-5] for motion of an axially symmetric pressure region. Analysis of dynamic deflection under a lumped load in shallow water was carried out in [6].

1. Let a thin elastic uniformly compressed film float on the surface of a homogeneous ideal incompressible fluid of thickness H = const. A pressure region is displaced over the film with constant velocity v

$$p = p_0 f(x_1, y),\ x_1 = x + vt,\ v = \text{const}. \tag{1.1}$$

We consider the bending gravitational film oscillations excited in this case and the fluid wave perturbations in the near zone of the pressure region.

Under the assumptions of the linear theory the problem consists of solving the Laplace equation

Sevastopol'. Translated from Zhurnal Prikladnoi Mekhaniki i Tekhnicheskoi Fiziki, No. 3, pp. 158-166, May-June, 1989. Original article submitted February 2, 1988.

0021-8944/89/3003-0490$12.50

$$\Delta\varphi = 0,\ -H < z < 0,\ -\infty < x < \infty,\ -\infty < y < \infty \tag{1.2}$$

with boundary

$$D_1\nabla^4\zeta + Q_1\nabla^2\zeta + \varkappa_1\zeta_{tt} + \zeta + \frac{1}{g}\varphi_t = -\frac{p}{\rho g},\ z = 0,$$
$$\varphi_z = 0,\ z = -H,\ \zeta_t = \varphi_z,\ z = 0 \tag{1.3}$$

and initial

$$\varphi(x, y, z, 0) = \zeta(x, y, 0) = 0 \tag{1.4}$$

conditions, where $D_1 = D/\rho g$, $Q_1 = Q/\rho g$, $\varkappa_1 = \rho_1 h/\rho g$, $D = Eh^3/12(1-\mu^2)$, $\nabla^2 = \partial^2/\partial x^2 + \partial^2/\partial y^2$, $\nabla^4 = (\nabla^2)^2$; ρ is the fluid density; E, h, ρ_1, and μ are the normal elasticity modulus, the thickness, density, and Poisson coefficient of the film, and Q is the compressing force.

Transforming to the coordinate system x_1, y, z fixed in the moving pressure region, and applying Fourier integral transforms over the horizontal coordinates x_1, y and the Laplace transform in time t, from (1.1)-(1.4) we obtain for an axially symmetric pressure distribution

$$\zeta = \frac{a}{8\pi^2}\int_0^\infty f_0(r)\,J(r, R, \gamma)\,dr,\quad J = \int_{-\pi/2}^{3\pi/2}\psi(r, \theta)\,e^{i[rR\cos(\theta-\gamma)]}\,d\theta,$$
$$\psi = \frac{2}{\Delta_1\Delta_2} - \frac{1}{\tau\Delta_1}e^{-i\Delta_1 t} + \frac{1}{\tau\Delta_2}e^{-i\Delta_2 t},\ a = \frac{p_0}{\rho g},\ \tau = [l(r)M(r)]^{1/2},$$
$$M = rg(1 + \varkappa_1 rg\ \mathrm{th}\ rH)^{-1}\ \mathrm{th}\ rH,\ l = D_1r^4 - Q_1r^2 + 1,$$
$$f_0 = rf^*(r)M(r),$$
$$\Delta_j = rv\cos\theta + \delta_j\tau,\ \delta_j = (-1)^j,\ x_1 = R\cos\gamma,\ y = R\sin\gamma,$$
$$R^2 = x^2 + y^2,\ m = r\cos\theta,\ n = r\sin\theta,\ r^2 = m^2 + n^2$$

[$f^*(r)$ is the Fourier transform of the function f(R)].

The integrand function $\psi(r, \theta)$ has no singularities on the integration path over θ for any $r \geq 0$, since the possible singularities of the separate terms, being the real roots of the equations $\Delta_1 = 0$, $\Delta_2 = 0$, cancel each other. Therefore, according to the Gauchy theorem, the original integration path along the real axis from $\theta = -\pi/2$ to $\theta = 3\pi/2$ can be deformed into the path L_0, bypassing in the complex plane the roots $\theta_{1,2} = \mp\arccos\tau_0$, $\tau_0 = \tau/(rv)$ of the equation $\Delta_1 = 0$ by small semicircles over which $\mathrm{Re}(i\Delta_1) > 0$, and the roots $\theta_{3,4} = \pi \mp \arccos\tau_0$ of the equation $\Delta_2 = 0$ by semicircles, on which $\mathrm{Re}(i\Delta_2) > 0$. We now rewrite J in the form

$$J = J_0 - J_{01} - J_{02},\ J_0 = \int_{L_0}\Phi_0(r, \theta)\,d\theta,\ J_{0j} = \int_{L_{0j}}\Phi_{0j}(r, \theta)\,d\theta,$$
$$\Phi_0 = \frac{2}{\Delta_1\Delta_2}\exp[irR\cos(\theta - \gamma)],\ \Phi_{0j} = \frac{1}{\tau\Delta_j}\exp(-i\Delta_j t),$$

where L_{01} bypasses only the points $\theta_{1,2}$, and L_{02} – the points $\theta_{3,4}$. Since $J_{1,2}$ tends to zero for $t \to \infty$ for any fixed R, it is obvious that J_0 characterizes the established motion, whose treatment is restricted in what follows by the condition $Q_1 < 2\sqrt{D_1}$, necessary for film stability.

2. If $v < v_0$ [$v_0 = \tau(r_0)/r_0$, where r_0 is the only positive root of the equation $\tau' = \tau/r$], then L_0 coincides with the real axis segment from $\theta = -\pi/2$ to $\theta = 3\pi/2$, so that in the given case $\Delta_1 \neq 0$ and $\Delta_2 \neq 0$. The integrand function in the expression for ζ also has no singularities in r, which makes it possible to investigate ζ numerically.

Let $v_0 < v < \sqrt{gH}$. We represent ζ in the form

$$\zeta = \frac{a}{8\pi^2}(\zeta_1 + \zeta_2 + \zeta_3),$$

$$\zeta_1 = \int_0^{r_1} f_0(r)\,J_0\,dr,\ \zeta_2 = \int_{r_1}^{r_2} f_0(r)\,J_0\,dr,\ \zeta_3 = \int_{r_2}^{\infty} f_0(r)\,J_0\,dr$$

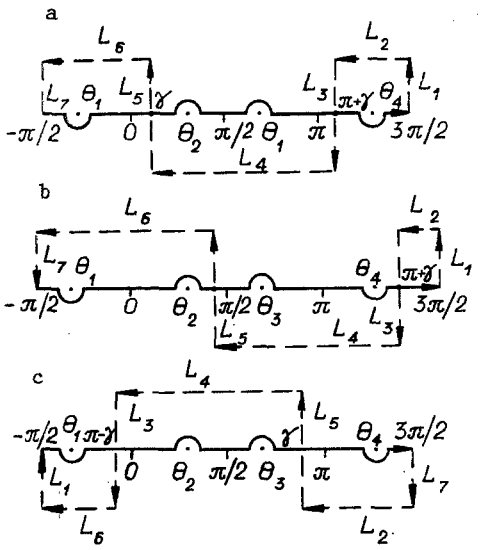

Fig. 1

(r_{12} are the real roots of the equation $\tau - rv = 0$). For $0 < r < r_1$, $r_2 < r < \infty$, J_0 has no singularities in θ. In this case, as well as for $v < v_0$, let L_0 coincide with a segment of the real axis. Then ζ_1 and ζ_3 have no singularities in r, except the edge integration points r_1 and r_2. Consequently, the integrals ζ_1 and ζ_3 can be evaluated numerically.

For $r_1 < r < r_2$ the path L_0 in the integral J_0 bypasses the points θ_1 and θ_4 in the lower, and the points θ_2 and θ_3 in the upper half-planes. We represent ζ_2 in the form

$$\zeta_2 = \zeta_2^* - \zeta_2^0, \quad \zeta_2^* = \int_{r_1}^{r_2} f_0(r) \int_{L^*} \Phi_0(r, \theta)\, d\theta\, dr,$$

$$\zeta_2^0 = \sum_{k=1}^{7} J_k, \quad J_k = \int_{r_1}^{r_2} f_0(r) \int_{L_k} \Phi_0(r, \theta)\, d\theta\, dr$$

(L^* is a closed contour, formed by L_0 and by the contours L_k, on which $\mathrm{Re}\,[irR\cos(\theta - \gamma)] \leq 0$). The choice of L^* depends on the angle γ. For $0 \leq \gamma < \theta_2$, $\theta_2 \leq \gamma \leq \theta_3$, $\theta_3 < \gamma \leq \pi$ the contour L^* is illustrated in Fig. 1a-c, respectively, where L_0 is characterized by the solid line, and L_k by the dashed line. Following application of Cauchy's theorem, we find

$$\zeta_2^* = -2\pi (I_1 + I_2),$$

$$I_1 = \begin{cases} \displaystyle\int_{r_1}^{r_2} \Phi_1(r)\, dr, & 0 \leqslant \gamma \leqslant \pi - \theta_0, \\ \left[\displaystyle\int_{r_1}^{r_1^*} \Phi_1(r)\, dr + \int_{r_2^*}^{r_2} \Phi_1(r)\, dr \right], & \pi - \theta_0 < \gamma \leqslant \pi, \end{cases}$$

$$I_2 = \begin{cases} \displaystyle\int_{r_1^*}^{r_2^*} \Phi_2(r)\, dr, & 0 \leqslant \gamma < \theta_0, \\ 0, & \theta_0 \leqslant \gamma \leqslant \pi, \end{cases}$$

$$\Phi_{1,2} = \frac{f_0(r)}{\tau \sqrt{(vr)^2 - \tau^2}} \sin\left[\frac{R}{v}\left(\tau\cos\gamma \mp \sqrt{(rv)^2 - r^2}\sin\gamma\right)\right],$$

$$\theta_0 = \max_{r_1 < r < r_2} \arccos \tau_0.$$

Here $r_{1,2}^*(\gamma)$ are the roots of the equation $\gamma = \theta_2(r)$ if $0 < \gamma < \theta_0$, and of the equation $\gamma = \theta_3(r)$ for $\pi - \theta_0 < \gamma < \pi$. The functions $\Phi_{1,2}$ and I_k have no singularities in r, besides the integrated ones at r_1, r_2.

From the condition $\mathrm{Re}\,[irR\cos(\theta-\gamma)]<0$ it follows that when the imaginary part of θ in the complex plane tends to infinity (Fig. 1) we obtain $J_2=J_4=J_6=0$. Since $\Phi_0(r,\theta)=\Phi_0(r,\theta+2\pi)$, and L_1 and L_7 are oppositely directed, we then have $J_1+J_7=0$.

After replacing $\omega=i[(\pi+\gamma)-\theta]$ in the integral J_3 and $\omega=i(\theta-\gamma)$ in J_5, we obtain

$$J_3+J_5=-\int_{r_1}^{r_2}(\tau v)^{-1}f_0(r)(u_1^*+u_2)\,dr,$$

$$u_n(r,\gamma,R)=(-1)^n\int_{-\infty}^{\infty}\frac{\sin(rR\,\mathrm{ch}\,\omega)}{\mathrm{ch}(\omega-i\gamma)+(-1)^n\tau_0}\,d\omega,\quad n=1,2.$$

We transform u_n to the form

$$u_n=2(-1)^n\int_0^{\infty}\frac{\sin(rR\,\mathrm{ch}\,\omega)\left[\mathrm{ch}\,\omega\cos\gamma+(-1)^n\tau_0\right]}{\left[\mathrm{ch}\,\omega\cos\gamma+(-1)^n\tau_0\right]^2+(\mathrm{sh}\,\omega\sin\gamma)^2}\,d\omega.$$

Hence we have, after substituting $u=\cosh\omega$,

$$u_n=2(-1)^n\int_1^{\infty}\frac{u_0\sin(rRu)}{\sqrt{u^2-1}\left[u_0^2+(u^2-1)\sin^2\gamma\right]}\,du,\ u_0=u\cos\gamma+(-1)^n\tau_0. \tag{2.1}$$

Taking into account that

$$u_0^2+(u^2-1)\sin^2\gamma=\left[u+(-1)^n\tau_0\cos\gamma\right]^2-(1-\tau_0^2)\sin^2\gamma,$$

we find from (2.1), by the method of undetermined coefficients,

$$u_1+u_2=(1-\tau_0^2)^{-1/2}\sum_{m=1}^{2}\sum_{n=1}^{2}(-1)^{m+n+1}\sin Q_{mn}\int_1^{\infty}\Phi^*\,du,$$

$$\Phi^*=\sin(rRu)\,(u^2-1)^{-1/2}\,(u-\cos Q_{mn})^{-1},$$

$$Q_{mn}=\gamma+(-1)^{m+n}\arccos\tau_0+\left[1+(-1)^n\right]\frac{\pi}{2}.$$

Since $\frac{1}{\sqrt{2}}\int\frac{du}{\sqrt{u-1}\,(u-\cos Q_{mn})}=\frac{\sqrt{2}}{\sqrt{1-\cos Q_{mn}}}\,\mathrm{arctg}\sqrt{\frac{u-1}{1-\cos Q_{mn}}}$ and $\sqrt{2}/\sqrt{1-\cos Q_{mn}}=1/|\sin(Q_{mn}/2)|$, by replacing $\sqrt{u^2-1}$ by $\sqrt{2}\sqrt{u-1}$ in a small ε-neighborhood of the lower limit, we obtain, by integration by parts,

$$\sin Q_{mn}\int_1^{u_0^*}\Phi^*\,du\approx\sqrt{2(1+\cos Q_{mn})}\,A(r,\varepsilon),$$

$$A=(A_1-A_2)\,\mathrm{sign}\,A_3,\quad A_1=\sin\left[rR(1+\varepsilon)\right]\mathrm{arctg}\sqrt{\varepsilon/(1-\cos Q_{mn})},$$

$$A_2=rR\int_1^{u_0^*}\cos(rRu)\,\mathrm{arctg}\sqrt{(u-1)/(1-\cos Q_{mn})}\,du,$$

$$A_3=(-1)^n\sqrt{1-\tau_0^2}\cos\gamma+(-1)^m\tau_0\sin\gamma,\ u_0^*=1+\varepsilon.$$

The integrals A_2 and $\int_{u_0^*}^{\infty}\Phi^*\,du$, and consequently also $J_3+J_5=J_3$ can be evaluated numerically. Thus, the problem of determining ζ has been reduced to numerical integration of the expressions for ζ_1, ζ_3, and I_k $(k=1,2,3)$.

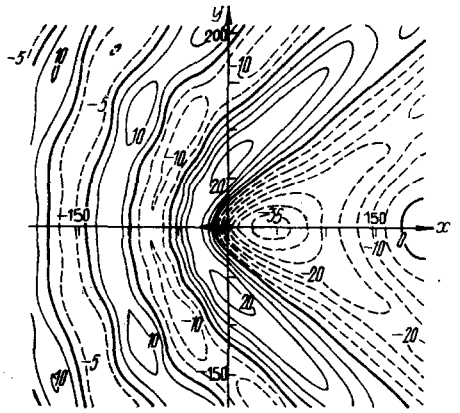

Fig. 2

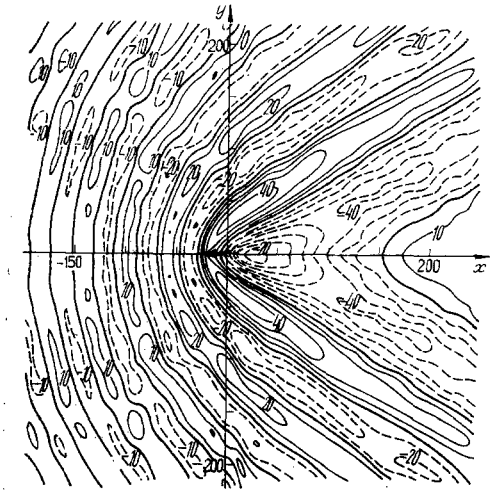

Fig. 3

TABLE 1

k	u_k^*	a_k	b_k	p_k	q_k
1	1,06	1,04	3,5007	831,52	—44,617
2	1,15	1,10	2,1822	84,615	—11,430
3	1,46	1,30	1,2059	5,5380	—2,2681

The integral $\int_{u_0^*}^{\infty} \Phi^* du$ can be evaluated approximately analytically, replacing $(u^2 - 1)^{-1/2}$ at the finite segments of integration paths $[u_0^*, u_1^*]$, $[u_1^*, u_2^*]$, and $[u_2^*, u_3^*]$ by expressions of the form $p_k(u - a_k)^2 + q_k(u - a_k) + b_k$. On the segment from u_3^* to ∞ the function $\sqrt{1 - u^{-2}}$ is replaced for $1/u^2 \ll 1$ by the first two terms of its Taylor series expansion in powers of $1/u^2$. The lengths of the integration segments and the coefficients p_k, q_k, a_k, and b_k are selected in such a manner that the approximation error not exceed a given one.

As a result of the approximation suggested we obtain

$$\int_{u_{k-1}^*}^{u_k^*} \Phi^* du \approx A_4(u_k^*) - A_4(u_{k-1}^*), \quad A_4 = A_{41} + A_{42},$$

$$A_{41} = p_k(rR)^{-2} \sin(rRu) - [p_k(u - a_k - \beta_k) + q_k](rR)^{-1} \cos(rRu),$$

$$A_{42} = (p_k\beta_k^2 - q_k\beta_k + b_k)[\sin\beta_0 \operatorname{Ci}(rR\beta) + \cos\beta_0 \operatorname{Si}(rR\beta)],$$

$$\beta_k = a_k - \cos Q_{mn}, \quad \beta_0 = rR\cos Q_{mn}, \quad \beta = u - \cos Q_{mn},$$

$$\int_{u_3^*}^{\infty} \Phi^* du = \sum_{l=1}^{2} F_l(r), \text{ где } F_l = [2\cos Q_{mn} + (-1)^l \sqrt{2}]^{-1} A_5$$

for $\cos Q_{mn} \neq (-1)^{l+1} \frac{1}{\sqrt{2}}$ and $F_1 = A_6$ for $\cos Q_{mn} = (-1)^{l+1} \frac{1}{\sqrt{2}}$. Here,

$$A_5 = \left(\frac{\pi}{2} - \operatorname{Si}\beta_4\right)\cos\beta_0 - \operatorname{Ci}\beta_4 \sin\beta_0 - \left(\frac{\pi}{2} - \operatorname{Si}\beta_5\right)\cos\frac{rR}{\sqrt{2}} - (-1)^l \operatorname{Ci}\beta_5 \sin\frac{rR}{\sqrt{2}};$$

$$A_6 = \frac{\sin(u_3^* rR)}{2u_3^* + (-1)^l\sqrt{2}} + \frac{rR}{2}\left[(-1)^l\left(\frac{\pi}{2} - \operatorname{Si}\beta_5\right)\sin\frac{rR}{\sqrt{2}} - \operatorname{Ci}\beta_5\cos\frac{rR}{\sqrt{2}}\right];$$

$$\beta_4 = rR(u_3^* - \cos Q_{mn}); \quad \beta_5 = rR\left(u_3^* + \frac{(-1)^l}{\sqrt{2}}\right).$$

If $v > \sqrt{gH}$, the equation $\tau - rv = 0$ has only one real root $r = r_2$. In this case, $\zeta = a/8\pi^2(\zeta_2 + \zeta_3)$, besides, the lowest limit in the integrals ζ_2, ζ_2^*, and J_k will vanish, and the expressions I_k acquire the form

$$I_1 = \begin{cases} \int_0^{r_2} \Phi_1(r)\,dr, & 0 \leqslant \gamma \leqslant \pi - \theta_0, \\ \left[\int_0^{r_1^*} \Phi_1(r)\,dr + \int_{r_2^*}^{r_2} \Phi_1(r)\,dr\right], & \pi - \theta_0 < \gamma < \pi - \theta^*, \\ \int_{r_2^*}^{r_2} \Phi_1(r)\,dr, & \pi - \theta^* \leqslant \gamma \leqslant \pi, \end{cases}$$

$$I_2 = \begin{cases} \int_0^{r_2^*} \Phi_2(r)\,dr, & 0 \leqslant \gamma \leqslant \theta^*, \\ \int_{r_1^*}^{r_2^*} \Phi_2(r)\,dr, & \theta^* < \gamma < \theta_0, \\ 0, & \theta_0 \leqslant \gamma \leqslant \pi, \end{cases}$$

where $\theta^* = \arccos(\sqrt{gH}/v)$. The expression for I_3 remains the former one. However, when it is calculated by using the approximation suggested, it must be kept in mind that $A_{41}(u_k^*) - A_{41}(u_{k-1}^*) = 0$ at the point $r = 0$.

3. Numerical analysis of the perturbation was carried out for an icy film [6, 7] in the case of a lumped load of a δ-function type $f(x_1, y) = \delta(x_1/H)\delta(y/H)$ for $E = 3 \cdot 10^9$ N·m^{-2}, $\rho_1 = 870$ kg·m^{-3}, $\rho = 10^3$ kg·m^{-3}, $\mu = 0.34$. The film thickness was taken to be 1 and 2 m, and the quantity Q_1, characterizing ice compression, was assumed equal to 0, $\sqrt{D_1}$, $1.5\sqrt{D_1}$. The fluid depth was taken to be 10^3 m for $v < \sqrt{gH}$ and 30 m for $v > \sqrt{gH}$. In this case, the value of ε was assumed equal to 0.02. The coefficients p_k, q_k, b_k, a_k of the polynomials, approximating the function $(u^2 - 1)^{-1/2}$ with an error of 1.5% on the segments $[u_{k-1}^*, u_k^*]$, and the values of u_k^* ($k = 1, 2, 3$) were selected from Table 1.

The results of numerical calculations are shown in Figs. 2-5, where the isoline deviations from the unperturbed level are given in millimeters. For $v < \sqrt{gH}$ (Figs. 2-4) the load weight is $1.6 \cdot 10^6$ N, and for $v > \sqrt{gH}$ (Fig. 5), it is $1.44 \cdot 10^6$ N, corresponding to $2\pi p_0 = 10^2$ and 10^5 Pa. The partition scale over the coordinate scales in the figures is given in meters.

Analysis of the results of the numerical calculations showed that for pressure displacement velocities near zero the film deflection ζ has a nearly axially symmetric shape in the case $Q = 0$. The axial symmetry of the deflection breaks down with increasing velocity, but the symmetry relative to the coordinate axes is retained. In this case the depth of the deflection is maximum under the load. Local elevations are formed in front and behind the load, extended in the directions perpendicular to the course of the load. There also exists an extended deflection under the load in the same direction. The deflection curvature is maximum in front of the load and behind it, and minimum in the direction perpendicular to the drawing.

Local elevations also occur on both sides of the drawing. However, their height increases with load velocity substantially more slowly than the height subtended over the course. For v near v_0 the height of both elevations is less than 20% than the elevation height over the drawing. An increase in the ice thickness leads to a decrease, and an increase in the velocity v leads to an increase in the deflection depth and the formation of elevations over the drawing. The distance between the centers of the deflection base and the elevations over the drawing increases with ice thickness and decreases with v.

The spatial distribution of perturbation amplitudes in the fluid at a fixed depth is qualitatively the same as on the ice–water surface, but the damping of perturbation with depth above the drawing occurs more slowly than under it.

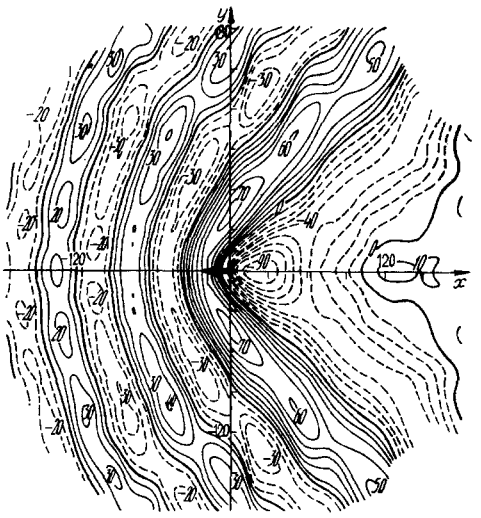

Fig. 4

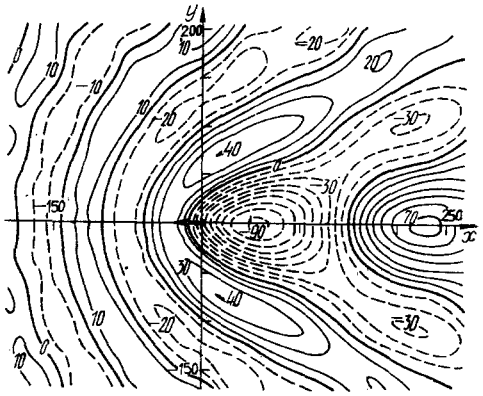

Fig. 5

The deflection topography variation under the effect of compression with fixed v is qualitatively the same as for the variation of load displacement velocity with Q = 0. The deflection depth and the elevation height at the drawing increase with compressing force and decrease with increasing tension. The distance between the centers of their bases varies in the opposite direction. For $v > v_0$ the symmetry of the film–fluid surface topography is retained only with respect to the pressure displacement drawing. The maximum deflection point is found now behind the load, being further removed from it with increasing v. The points of maximum deepening of deflection lines parallel to the drawing are also further removed in this case. The geometric locus of these points has a nearly hyperbolic distribution with a vertex on the drawing. The direction of deflection grooves makes with the drawing an angle near $\tan^{-1}[(v/v_0)^2 - 1]^{-1/2}$.

The wave perturbations in front and behind the deflection decay substantially more slowly with moving away from the load (approximately as $1/R^{1/2}$) than in the case $v < v_0$. The leading slope of the deflection is steeper than the trailing one. In front of the load the wave is substantially shorter than behind the loading. The deflection depth and the amplitudes of wave perturbations decrease with increasing v for $v > v_0$. The wavelength decrease in front of the load and increase behind it. The rates of variation of wavelengths and amplitudes behind the region of increasing v are substantially higher than in front of it.

For low excess velocities of v beyond v_0 the wave amplitudes are approximately equal in front of and behind the load. As for $v < v_0$, they decay monotonically along their crests. Further increase of v leads to the appearance of local extrema at the perturbation crests (depressions) in front of the load. The line joining the extrema in height (depth) is a branch of a hyperbola with a vertex at the maximum deflection point on the drawing. The ray direction of this branch depends on the velocity v. The larger v, the larger the angle formed by these rays with the direction of load motion. The deflection trough is extended in the wavy trail behind the pressure region, acquiring a weakly expressed hilly channel, i.e., the depth of the trough decreases nonmonotonically with distance from the drawing. The smooth illustration of the topography perturbation for this case is shown in Fig. 2 for $v = 0.3\sqrt{gH}$, h = 2 m, Q = 0.

We note that if v exceeds some value, denoted by v_1 in [4, 5], then wave structures are also acquired by both trough boundaries in the wavy trail. This is seen from the topography in Fig. 3 for h = 1 under the same conditions as in Fig. 2. We note that this effect is obviously due to the contribution of longitudinal waves of the type of marine waves, excited for $v > v_1$ [1, 3, 4].

For $v > \sqrt{gH}$, the wave perturbations are insignificant behind the deflection in the wake. In particular, for H = 30 m, h = 1 m, $v = 1.2\sqrt{gH}$, Q = 0 (Fig. 4) the crest heights in front of and behind the deflection are 70 and 10 mm, respectively. Besides, the first crest in front of the deflection acquires a clearly expressed wavy nature.

Analysis of the results of numerical calculations has also shown that a decrease in the film thickness for a fixed v value in each of the regions $v_0 < v < v_1$, $v_1 < v < \sqrt{gH}$,

$v > \sqrt{gH}$ leads to an increase in the deflection depth and amplitudes of maximum wave perturbations. Besides, the wave crests in front of the load become more hilly. This becomes obvious by comparing Figs. 2 and 3. Also possible is the appearance of substantial local elevations on both sides of the drawing behind the deflection with velocities in the region $v_0 < v < v_1$. The angle between the deflection trough and the drawing decreases behind the pressure region with decreasing film thickness.

Uniform compression increases the maximum depth of the deflection. The angle between the direction of the deflection trough and the abscissa axis decreases with increasing compressing force. The elevation behind a deflection with increasing Q is extended along the drawing, and narrows down in the transverse direction. Its height increases substantially in this case, which is possibly a consequence of superposition of excess, longitudinal and transverse marine waves, occurring near the drawing behind the load [4] for compressing forces exceeding the quantity Q* obtained in [2]. The structure of the deflection trough and the distribution of perturbation amplitudes along the troughs vary qualitatively in front of the load with increasing compressing force in the same manner as with increasing load displacement velocity. The perturbation topography for $Q = 1.5\sqrt{D_1}$, h = 2 m, $H = 10^3$ m, and $v = 0.2\sqrt{gH}$ is illustrated in Fig. 5.

The amplitudes of excess perturbations (in front of the load) decay with fluid depth more quickly than gravitational ones and those due to the deflection (behind the load). The damping of excess perturbations is enhanced with depth due to their decreasing length with increasing load displacement velocity, compressing force, and decreasing film thickness. This also leads to enhancement of different perturbation topographies in the fluid at a given depth and at the film–fluid surface. The point of maximum deviation from the unperturbed level at a fixed depth deviates more strongly from the load than the corresponding point of maximum film deflection. The hilly nature of excess perturbation crests and of deflection troughs are smoothed with increasing depth, in which case the points of maximum amplitude of excess perturbations are more removed from the plane of the drawing.

LITERATURE CITED

1. L. V. Cherkesov, Wave Hydrodynamics [in Russian], Naukova Dumka, Kiev (1980).
2. A. E. Bukatov, "Effect of a longitudinally compressed elastic film on nonestablished wave motion of a homogeneous fluid," Izv. Akad. Nauk SSSR, Mekh. Zhidk. Gaza, No. 5 (1980).
3. S. F. Dotsenko, "Gravitational-elastic and gravitational-capillary unstable marine waves," Izv. Akad. Nauk SSSR, Mekh. Zhidk. Gaza, No. 5 (1978).
4. A. E. Bukatov and A. A. Yaroshenko, "Effect of a uniformly compressed floating elastic film on the evolution of three-dimensional waves in a homogeneous fluid," Izv. Akad. Nauk SSSR, Mekh. Zhidk. Gaza, No. 6 (1984).
5. A. E. Bukatov and A. A. Yaroshenko, "Evolution of three-dimensional excess-gravitational waves during motion of a pressure region of varying intensity," Prikl. Mekh. Tekh. Fiz., No. 5 (1986).
6. D. E. Kheisin, Ice Sheet Dynamics [in Russian], Gidrometeoizdat, Leningrad (1967).
7. V. V. Bogorodskii and V. P. Gavrilo, Physical Properties of Ice; Contemporary Methods of Hydrology [in Russian], Gidrometeoizdat, Leningrad (1980).